Published in final edited form as:
Bioconjug Chem. 2011 August 17; 22(8): 1459–1472. doi:10.1021/bc200106p.

^{64}Cu-Labeled Phosphonium Cations as PET Radiotracers for Tumor Imaging

Yang Zhou and **Shuang Liu**
School of Health Sciences, Purdue University, 550 Stadium Mall Drive, West Lafayette, IN 47907, Phone: 765-494-0236

Shuang Liu: liu100@purdue.edu

Abstract

Alteration in mitochondrial transmembrane potential ($\Delta\Psi_m$) is an important characteristic of cancer. The observation that the enhanced negative mitochondrial potential is prevalent in tumor cell phenotype provides a conceptual basis for development of mitochondrion-targeting therapeutic drugs and molecular imaging probes. Since plasma and mitochondrial potentials are negative, many delocalized organic cations, such as rhodamine-123 and ^{3}H-tetraphenylphosphonium, are electrophoretically driven through these membranes, and able to localize in the energized mitochondria of tumor cells. Cationic radiotracers, such as ^{99m}Tc-Sestamibi and ^{99m}Tc-Tetrofosmin, have been clinically used for diagnosis of cancer by single photon emission computed tomography (SPECT) and noninvasive monitoring of the multidrug resistance (MDR) transport function in tumors of different origin. However, their diagnostic and prognostic values are often limited due to their insufficient tumor localization (low radiotracer tumor uptake) and high radioactivity accumulation in the chest and abdominal regions (low tumor selectivity). In contrast, the ^{64}Cu-labeled phosphonium cations represent a new class of PET (positron emission tomography) radiotracers with good tumor uptake and high tumor selectivity. This review article will focus on our recent experiences in evaluation of ^{64}Cu-labeled phosphonium cations as potential PET radiotracers. The main objective is to illustrate the impact of radiometal chelate on physical, chemical and biological properties of ^{64}Cu radiotracers. It will also discuss some important issues related to their tumor selectivity and possible tumor localization mechanism.

Keywords

^{64}Cu; phosphonium cations; tumor imaging and PET

Introduction

Early Detection of Cancer

Cancer is the second leading cause of death worldwide. The most prevalent forms of this disease are solid tumors of the lung, breast, prostate, colon and rectum.[1] Most cancer patients can survive for a long period of time after surgery, radiation and chemotherapy or a combination thereof if it can be detected at the early stage. Therefore, accurate early detection is highly desirable so that various therapeutic regimens can be given before tumors become widely spread. Many imaging modalities are currently available for early cancer detection. Ultrasonography (US), computed tomography (CT) and magnetic resonance imaging (MRI) can provide details of structural changes, variations in density and differences in proton content in tissues. However, it remains a significant challenge to use US, CT and MRI methods for molecular imaging of cancer. Nuclear medicine procedures using radiolabeled receptor ligands can provide the *in vivo* characterization of cellular

structure, and are able to monitor biological changes in tumor tissues at the cellular and molecular levels. A “fatal flaw” for most of the receptor-based target-specific radiotracers is that not all tumors over-express that specific receptor. Thus, it is of great benefit to develop a molecular imaging probe that could detect cancers by targeting a biomarker found in majority, if not all, of human cancer lesions.

Targeting Energized Mitochondria

Alteration in mitochondrial transmembrane potential ($\Delta \Psi_m$) is an important characteristic of cancer caused directly by mitochondrial dysfunction, such as DNA mutation and oxidative stress.[2–5] It has been reported that the mitochondrial transmembrane potential in carcinoma cells (regardless of the tumor origin) is significantly higher than that in normal epithelial cells.[6–11] For example, the difference in $\Delta\Psi_m$ between the colon carcinoma cell line CX-1 and the control green monkey kidney epithelial cell line CV-1 was approximately 60 mV (163 mV in tumor cells vs. 104 mV in normal cells). The observation that the enhanced negative mitochondrial potential is prevalent in tumor cell phenotype provides the conceptual basis for development of mitochondrion-targeting therapeutic pharmaceuticals and molecular imaging probes.[2–5, 12–25]

Measuring Mitochondrial Potential with Lipophilic Organic Cations

Mitochondrial potential measurement provides the most comprehensive reflection of mitochondrial bio-energetic function primarily because it directly depends on the proper integration of diverse metabolic pathways that converge at mitochondria. Since both plasma and mitochondrial potentials are negative, many delocalized cationic molecules with appropriate structural features are electrophoretically driven through these transmembranes, and tend to accumulate inside the energized mitochondria of tumor cells.[2–5, 12–17] This is exemplified by the use of rhodamine-123 and ^{3}H-tetraphenylphosphonium (^{3}H-TPP) for measurement of mitochondrial potential in tumor cells on the basis of their intracellular and mitochondrial concentration.[6–10, 13, 15, 16] In addition, rhodamine derivatives have also been used as fluorescent probes for optical imaging of tumors n animal models.[18–25]

Imaging Tumors with Cationic Radiotracers

Cationic radiotracers, such as ^{99m}Tc-Sestamibi and ^{99m}Tc-Tetrofosmin, were developed as radiotracers for myocardial perfusion imaging by single photon emission computed tomography (SPECT).[26–31] It was found that these cationic radiotracers are also able to localize in tumors due to the increased negative plasma and mitochondrial potential in tumor cells as compared to normal cells of surrounding tissues.[32–42] ^{99m}Tc-Sestamibi and ^{99m}Tc-Tetrofosmin have been clinically used for diagnosis of cancer and noninvasive monitoring of the tumor multidrug resistance (MDR) transport function.[33, 36–42] However, their diagnostic and prognostic values are often limited due to their insufficient tumor localization and high radioactivity accumulation in the chest and abdominal regions.

Radiolabeled Phosphonium Cations as Radiotracers

More than 20 years ago, radiolabeled quaternary ammonium, phosphonium and arsonium cations were studied as perfusion radiotracers for heart imaging.[43, 44] Recently, several groups proposed to use radiolabeled triphenylphosphonium, such as 4-(^{18}F-benzyl)triphenylphosphonium (^{18}F-BzTPP), cations as PET radiotracers for myocardial perfusion and tumor imaging.[45–52] It has been reported that ^{3}H-tetraphenylphosphonium (^{3}H-TPP) has better tumor uptake than ^{99m}Tc-Sestamibi;[53] but its tumor selectivity is poor with tumor/heart ratios «1.0. Since ^{3}H-TPP is not suitable for PET imaging, the ^{11}C-labeled TPP cation has been proposed as the alternative.[45, 46] In addition, the high uptake of ^{18}F-BzTPP in the heart and liver may impose a significant challenge for its application in

diagnosis of cancer in chest and abdominal regions. Even though biodistribution and imaging studies in small animals[45, 52] and dogs[45, 46, 49] have clearly demonstrated the utility of ^{11}C and ^{18}F-labeled TPP cations for imaging heart and tumors by PET, the combination of short half-life of ^{11}C ($T_{1/2}$ = 20.4 min, 98% abundance) and ^{18}F ($T_{1/2}$ = 110 min, 97% abundance) with their poor availability and high cost of infrastructure makes it very difficult to use ^{11}C and ^{18}F-labeled TPP cations for PET studies of cancer patients in most of the clinic settings. Therefore, there is an urgent need for new and better PET radiotracers that can be readily prepared, have high tumor-selectivity, and are able to provide the information of the tumor mitochondrial function in a noninvasive fashion.

About This Review

Many review articles appeared covering the nuclear medicine applications of cationic radiotracers for tumor imaging and noninvasive monitoring of tumor MDR transport function by SPECT or PET.[36–42] This article is not intended to be an exhaustive review of current literature on cationic radiotracers and their nuclear medicine applications. Instead, it will focus on our recent experiences in evaluations of ^{64}Cu-labeled phosphonium cations as highly tumor-selective PET radiotracers. This review will also discuss some important issues related to their tumor selectivity and localization mechanism. The main objective is to illustrate the impact of bifunctional chelators (BFCs) and radiometal chelate on physical, chemical and biological properties of ^{64}Cu-labeled phosphonium cations. It is very important to note that the mitochondrion-targeted radiotracers described in this article are not intended to measure the exact mitochondrial potential in tumor cells as ^{3}H-TPP and the rhodamine derivatives are used for many *in vitro* assays.[6–10, 13, 15, 16] Considering the heterogeneity of tumor cells in different regions of the same tumor tissue and among different types of tumors, these mitochondrion-targeted radiotracers are designed to noninvasively determine the contrast between the tumor and surrounding normal tissues.

Radiotracer Design and Synthesis

Characteristics of Optimal Radiotracers

For a new tumor-specific radiotracer to be successful, it must show clinical indications for high-incidence tumors (breast, lung and prostate cancers). The radiotracer should have high tumor uptake and target-to-background (T/B) ratios in a short period of time postinjection (p.i.). To achieve this goal, the radiotracer should have a rapid blood clearance to minimize background radioactivity. Since most high-incidence tumors occur in the chest and abdominal regions, renal excretion is needed to avoid excessive radioactivity accumulation in the gastrointestinal tract, which might interfere with interpretation of tumor radioactivity.

Radiotracer Design

Figure 1 shows selected phosphonium cations, bifunctional chelators (BFCs) and PKM (pharmacokinetic modifying) linkers. The phosphonium cation serves as a targeting moiety to carry ^{64}Cu into the energized mitochondria of tumor cells. The BFC is required for chelation of ^{64}Cu. PKM linkers are used to improve pharmacokinetics of ^{64}Cu radiotracers. In principle, the ^{64}Cu-labeled phosphonium cations should be useful for imaging most tumors, if not all, since the higher negative mitochondrial potential is prevalent in tumor cell phenotypes.[47–53] Their high tumor selectivity provides a unique opportunity to develop radiotracers that are sensitive to the early change in tumor mitochondrial potential. Successful development of such a radiotracer will be beneficial for the early detection of cancer. It must be noted that the ^{64}Cu-labeled phosphonium cations are significantly different from their ^{18}F-analogs with respect to their physical, chemical and biological properties. Replacing ^{18}F with a ^{64}Cu-BFC chelate has significant impact on the biological

characteristics of phosphonium cations due to its large size, hydrophilicity and the change in overall molecular charge.

Why ^{64}Cu or ^{62}Cu?

^{64}Cu has a half-life of 12.7 h and a β^+ emission (18%, E_{max} = 0.655 MeV). Despite its low β^+ abundance, the long half-life makes it feasible to prepare, transport and deliver the ^{64}Cu radiotracer for its clinical applications.[54, 55] Recent breakthroughs in production of ^{64}Cu with high specific activity have made it more available to small institutions without the on-site cyclotron facilities.[54] Thus, ^{64}Cu is a viable alternative to ^{18}F for research programs that wish to incorporate high sensitivity and high spatial resolution of PET, but cannot afford to maintain the expensive radionuclide production infrastructure. ^{62}Cu is a generator-produced radionuclide. Its 9.7 min half-life allows the repeated dosing without imposing a significant radiation burden to the patient. Copper radionuclides, related radiochemistry and nuclear medicine applications of ^{64}Cu-radiotracers have been reviewed extensively.[54–60] We have evaluated several metallic radionuclides (^{99m}Tc, ^{64}Cu and ^{111}In) for radiolabeling of phosphonium cations. It was found that only the ^{64}Cu-labeled phosphonium cations are able to localize in U87MG glioma tumors with long tumor retention while the corresponding ^{99m}Tc and ^{111}In radiotracers tend to have significant tumor washout. Since ^{64}Cu and ^{62}Cu share identical coordination chemistry, ^{62}Cu-labeled phosphonium cations are expected to have the same biodistribution characteristics as their ^{64}Cu analogs.

Bifunctional Chelators for ^{64}Cu Chelation

Due to the d^9 configuration, Cu(II) complexes are kinetically labile. BFCs for $^{62/64}$Cu-labeling are often macrocyclic and form Cu(II) complexes with high thermodynamic stability and kinetic inertness.[61–76] Since most phosphonium cations are relatively small, the optimal BFCs would be those which form low molecular weight ^{64}Cu chelates. That is why DO3A (1,4,7,10-tetraazacyclododecane-1,4,7-tetraacetic acid), DO2A (1,4,7,10-tetraazacyclododecane-1,4-diacetic acid), DOTA (1,4,7,10-tetraazacyclododecane-1,4,7,10-tetraacetic acid), and NOTA (1,4,7-tritazacyclononane-1,4,7-triacetic acid) are used as the BFCs for ^{64}Cu-labeling of phosphonium cations.[61–64] These BFCs are able to form anionic or neutral ^{64}Cu chelates so that the overall molecular charge of the ^{64}Cu radiotracers is either neutral or positive under physiological conditions.

Synthesis of Conjugated Organic Cations

DO3A conjugates were readily prepared according to Chart I by reacting the DO3A(OBu-t)$_3$ with the respective bromide in DMF in the presence of sodium carbonate.[61, 63, 64] Hydrolysis of the t-butyl ester in hydrochloric acid gave the expected DO3A conjugates (**1**: DO3A-pn-TPP; **2**: DO3A-bn-TPP; **3**: DO3A-xy-TPP; **4**: DO3A-xy-TPA; **5**: DO3A-xy-mTPP; and **6**: DO3A-xy-TPEP). DO2A-xy-TPP (**7**) and DO2A-(xy-TPP)$_2$ (**8**) were prepared according to Chart II by N-alkylation of DO2A(OBu-t)$_2$ with 4-(bromomethylbenzyl)triphenylphosphonium.[63] DOTA-Bn-xy-TPP (**9**), DOTA-Bn-xy-TPEP (**10**), NOTA-Bn-xy-TPP (**11**) and NOTA-Bn-xy-TPEP (**12**) were prepared according to Chart III.[56] The key intermediates were (4-(aminomethyl)benzyl)(2-(diphenylphosphoryl)ethyl)diphenylphosphonium and 4-aminomethylbenzyl)triphenylphosphonium.[63, 64] Conjugates **1** – **12** were synthesized to explore the impact of phosphonium moiety, linker and BFCs on the biodistribution and excretion kinetics of their corresponding ^{64}Cu radiotracers.

Coordination Chemistry of DO3A-Conjugated TPP

Solid State Structures

To understand coordination chemistry of DO3A-conjugated phosphonium cations, we prepared complexes In(**3**)$^+$ and Ga(**3**)$^+$ as model compounds for ^{111}In(**3**)$^+$ and ^{68}Ga(**3**)$^+$, respectively, and Cu(**3**) as the model for ^{64}Cu(**3**). Mn(**3**) was prepared because of its similarity to Cu(**3**) with respect to molecular charge.[62] Despite their difference in overall molecular charge, In(**3**)$^+$ and Mn(**3**) have almost identical solid state structures with DO3A bonding to In(III) and Mn(II) in a monocapped octahedral coordination geometry (Figure 2).[62] Because of the smaller size of Ga(III), DO3A in Ga(**3**)$^+$ is only hexadentate with four amine-N and two carboxylate-O atoms bonding to Ga(III) in a distorted octahedral coordination geometry (Figure 2). One carboxylic acid group in DO3A is deprotonated in order to balance the positive charge of Ga(III).[62] Since the ionic radius of Cu(II) is close to that of Ga(III), it is reasonable to believe that the coordinated DO3A in Cu(**3**) is most likely hexadentate, as observed in Cu(DO3A),[77] with one acetate group being deprotonated to balance the cationic charge from TPP.

Solution Structures

Since ^{64}Cu(**3**) and ^{111}In(**3**)$^+$ are used as radiotracers in biological systems, it is necessary to study their solution properties (structure, isomerism and stability) in aqueous solution. On the basis of HPLC concordance experiments (Figure 3), it was concluded that ^{111}In(**3**)$^+$ and In(**3**)$^+$ have the same composition due to their identical HPLC retention times.[62] In(**3**)$^+$ remains symmetrical in aqueous solution with no dissociation of acetate chelating arms.[62] The presence of a single peak in the region of interest (Figure 3) suggests that they exist in solution as a single or “averaged” species. The HPLC retention times for In(**3**)$^+$ and Ga(**3**)$^+$ are almost identical (14.5 and 14.7 min, respectively); but they are significantly shorter than that of Mn(3) (16.8 min) and Cu(**3**) (17.2 min). Obviously, Ga(**3**)$^+$ and In(**3**)$^+$ with the +1 overall molecular charge are more hydrophilic than Mn(**3**) in its Zwitterion form.[62] The HPLC retention time of Mn(**3**) (16.8 min) is close to that of Cu(**3**) (17.2 min) under identical chromatographic conditions (Figure 3), suggesting that Cu(**3**) may also exist in solution as its Zwitterion form.[62–64] However, it is unclear if the two acetate chelating arms in ^{64}Cu(**3**) remains coordinated in solution. Because of its low concentration in the blood circulation, it is quite possible that ^{64}Cu-DO3A in ^{64}Cu(**3**) might become 4-coordinated with a square planar coordination sphere. The lower pH value (pH = 4.5 – 5.0) inside tumor cells as compared to normal cells (pH = 6.5 – 7.4) also makes it easier for the two acetate chelating arms to become dissociated from ^{64}Cu. This conclusion is supported by the fact that ^{64}Cu(**6**) underwent extensive tranchelation in the liver,[64] and completely consistent with the instability of the ^{64}Cu-DOTA chelate.[78–82]

Biological Evaluation

Biodistribution Characteristics

More than 25 ^{64}Cu-labeled phosphonium cations have been evaluated for their biodistribution characteristics and excretion kinetics in athymic nude mice bearing U87MG human glioma xenografts.[61, 63, 64] We were interested in this tumor-bearing animal model because the U87MG human glioma cell line has been used to evaluate the cellular uptake kinetics of ^{99m}Tc-Sestamibi and ^{99m}Tc-Tetrofosmin[83] due to its lack of MDR1 P-glycoprotein (MDR1 Pgp) expression.[84, 85] Western blotting studies also showed that the xenografted U87MG glioma tissues have little expression of MRP1, MRP2 and MRP4.[65] Figure 4 compares ^{99m}Tc-Sestamibi and three ^{64}Cu-labeled phosphonium cations for their uptake in the tumor, heart, liver and muscle, as well as tumor/heart and tumor/lung ratios. ^{99m}Tc-Sestamibi was used for comparison purposes since it has been clinically used

for tumor imaging and monitoring of the tumor MDR transport function.[36–42] The most striking difference is that all ^{64}Cu radiotracers have the heart uptake <0.6% ID/g while the heart uptake of ^{99m}Tc-Sestamibi was >15% ID/g over the 2 h period. As a result, ^{64}Cu radiotracers have the tumor/heart ratios much better than that of ^{99m}Tc-Sestamibi. The muscle uptake of ^{99m}Tc-Sestamibi was high (~5 %ID/g), whereas the muscle uptake of ^{64}Cu radiotracers was almost undetectable at >30 min p.i. Thus, the ^{64}Cu-labeled phosphonium cations have significant advantages over ^{99m}Tc-Sestamibi. The biodistribution of ^{64}Cu(**3**) and ^{64}Cu(**4**) was almost identical, suggesting the heteroatom (P vs. As) had very little impact on biodistribution of radiotracers.[61] ^{64}Cu(**3**) has the tumor uptake comparable to that of ^{64}Cu(**5**); but ^{64}Cu(**5**) has the lower liver uptake, indicating that the presence of methoxy groups improves the radiotracer liver clearance.[63] ^{64}Cu(**6**) had higher tumor uptake (Figure 4) than ^{64}Cu(**3**), but its liver uptake was much lower than that of ^{64}Cu(**3**).[64] This indicates that the high liver uptake of ^{64}Cu(**3**) is caused by TPP cation, not the *in vivo* instability of ^{64}Cu-DO3A. On the basis of tumor uptake and T/B ratios (Figure 4), we believe that TPEP has better tumor-targeting capability than TPP.

Impact of BFC

The tumor uptake of ^{64}Cu(**10**) is comparable to that of ^{64}Cu(**6**) at 30 – 60 min p.i. (Figure 5A); but its tumor/heart ratios are lower than those of ^{64}Cu(**6**), probably due to the benzene ring in ^{64}Cu(**10**).[64] Among ^{64}Cu-labeled phosphonium cations evaluated in the glioma model, ^{64}Cu(**11**) (Figure 5A) and ^{64}Cu(**12**) (Figure 5B) had very low tumor uptake, probably due to NOTA,[63, 64] which forms the Cu-NOTA chelate with better solution stability than that of Cu-DOTA.[75] The extra xy-TPP moiety in ^{64}Cu(**8**) also results in decreased tumor uptake (Figure 5B) and increased liver uptake, probably due to the +2 overall molecular charge and increased lipophilicity.[64] On the basis of biodistribution data, it becomes clear that (1) DO3A is the best BFC for ^{64}Cu-labeling of phosphonium cations; (2) NOTA-Bn has significant adverse effect on radiotracer tumor uptake; (3) DOTA derivatives might be useful BFCs if the aromatic benzene ring can be eliminated; and (4) the ^{64}Cu chelate should have the neutral or negative charge. The combination of relatively high tumor uptake and high T/B ratios makes ^{64}Cu(**6**) the most promising PET radiotracer for tumor imaging.[63, 64]

Impact of Metal Chelate

Figure 5C compares tumor uptake of ^{111}In(**3**), ^{64}Cu(**3**), ^{111}In(**6**) and ^{64}Cu(**6**). It is surprising that ^{64}Cu and ^{111}In radiotracers have such a significant difference in their tumor uptake. For example, both ^{64}Cu(**3**) and ^{64}Cu(**6**) have a steady increase in tumor uptake at 30 – 120 min p.i.[63, 64] while ^{111}In(**3**) and ^{111}In(**6**) had a significant tumor washout over the 2 h study period. At this moment, it is not clear what causes the difference between ^{111}In and ^{64}Cu-labeled phosphonium cations. It seems that the radiotracers with an octahedral solution structure and high *in vivo* stability (^{111}In-DO3A) tend to have much lower tumor uptake with shorter tumor retention time than those with a square-planar solution structure and relatively low *in vivo* stability (^{64}Cu-DO3A). More studies are still in progress to further define the role of radiometal chelates on the tumor uptake and tumor retention time of radiolabeled phosphonium cations.

MicroPET Imaging

Figure 6 illustrates microPET images for ^{64}Cu(**2**), ^{64}Cu(**3**) and ^{64}Cu(**6**) in athymic nude mice bearing U87MG glioma xenografts at 4 h p.i.[61, 63, 64] The tumors were clearly visualized with excellent T/B contrast. It is interesting to note that the tumor uptake of ^{64}Cu(**2**) was much lower than that of ^{64}Cu(**3**), but its background radioactivity was also much lower.[63] Therefore, all three ^{64}Cu radiotracers are useful for imaging MDR-negative tumors by PET.

Metabolism and ^{64}Cu-Transchelation in Liver

The metabolism studies showed that ^{64}Cu(**3**) and ^{64}Cu(**6**) are excreted via renal and hepatobiliary routes.[61, 64] There was no significant metabolism detectable for ^{64}Cu(**6**) in the feces sample at 120 min p.i. In contrast, only ~15% of ^{64}Cu(**3**) remains intact in feces during the same study period. The radio-HPLC analysis of the liver homogenate suggest that ^{64}Cu(**6**) underwent extensive ^{64}Cu-tranchelation in the liver.[64] While the identity of detected metabolites remains unknown, the radio-HPLC profile of ^{64}Cu(**6**) is very similar to that of ^{64}Cu-labeled TETA-Octreotide in rat liver homogenate.[81] Thus, it is reasonable to believe that these metabolites are likely caused by ^{64}Cu-transchelation from ^{64}Cu-DO3A chelate to the proteins, such as superoxide dismutase (SOD), which are abundant in the liver.[82]

Stability of ^{64}Cu-BFC Chelate and Radiotracer Liver uptake

Cu(II) has a d^9 configuration with coordination number being 4, 5 or 6 depending on chelator. The 4-coordinated Cu(II) complexes are normally square-planar while the square-pyramid coordination geometry is often seen in 5-coordinated Cu(II) complexes. In 6-coordinated Cu(II) complexes, the two apical donor atoms are weakly bonded to Cu(II) in a distorted octahedral arrangement due to John-Teller distortion. As discussed previously, BFCs for copper radionuclides are often macrocyclic chelators that form Cu(II) complexes with high thermodynamic stability and kinetic inertness.[55, 56] This was exemplified by early use of cyclam and cyclen derivatives for ^{67}Cu-labeling of monoclonal antibodies,[66] and further development of cross-bridged cyclam derivatives, such as CB-TE2A (2,2′-(1,4,8,11-tetraazabicyclo[6.6.2]hexadecane-4,11-diyl)diacetic acid).[76, 78–80] It was reported that ^{64}Cu-CB-TE2A had higher *in vivo* stability than ^{64}Cu-DOTA and ^{64}Cu-TETA.[76, 78–80] Since Cu(II) complexes are kinetically labile due to its d^9 configuration, the high liver uptake of ^{64}Cu radiotracers is often attributed to their *in vivo* instability, which leads to ^{64}Cu-transchelation from ^{64}Cu-BFC to copper-binding proteins, such as superoxide dismutase abundant in liver.[82] The metabolism of ^{64}Cu-labeled biomolecules and ^{64}Cu complexes of tetraazamacrocycles has been investigated extensively.[66, 76, 78–80] These studies clearly show that kinetic inertness of ^{64}Cu chelates is particularly important for *in vivo* stability of ^{64}Cu radiotracers. However, the results from our studies suggested that the high radiotracer liver uptake is mainly caused by phosphonium cations, not instability of ^{64}Cu-DO3A.[61, 63, 64] This conclusion is supported by the fact that ^{64}Cu(**7**) has significantly lower liver uptake than ^{64}Cu(**3**) even though ^{64}Cu-DO3A is expected to have better *in vivo* stability than ^{64}Cu-DO2A.[63] It is important to note that the tumor uptake of target-specific ^{64}Cu radiotracers is almost exclusively determined by receptor binding of targeting biomolecules. The BFCs for ^{64}Cu chelation should be those which form ^{64}Cu-BFC chelates with high kinetic inertness to minimize liver radioactivity accumulation. In contrast, the optimal BFC should be those which result in the ^{64}Cu radiotracer with high tumor uptake and the best T/B ratios since it has great impact on both tumor uptake and excretion kinetics of ^{64}Cu-labeled phosphonium cations. From this point of view, DO3A and DOTA are suitable BFCs for ^{64}Cu-labeling of phosphonium cations.

Tumor Localization Mechanism

Mitochondrial Potential: Driving Force for Tumor Localization

It is believed that mitochondrial potential is a major factor contributing to the tumor uptake of cationic radiotracers.[3, 13, 46, 47, 52] Various tumor cell lines exhibit differences in the number, size and shape of their mitochondria relative to normal control cells.[4] It has been reported that the mitochondria of rapidly growing tumors tend to be fewer in number and have fewer cristae than those from slowly growing tumors; the latter are larger and have characteristics closely resembling those of normal cells.[4] The main difference between

tumor cells and normal cells is mitochondrial potential (163 mV in carcinoma tumor cells vs. 104 mV in normal cells).[7–10] According to the Nernst equation, the ~60 mV increase in mitochondrial potential will result in approximately 10-fold more accumulation of cationic compounds in the energized mitochondria of tumor cells (Figure 7). It is this mitochondrial potential difference that provides the contrast (differential uptake of radiotracer) between tumor and surrounding normal tissues. In addition, the plasma potential (−30 – −60 mV) also pre-concentrates cationic species relative to the external medium, thus affecting their cytoplasma concentration and availability for the mitochondrial uptake.[13, 86–88]

Activation Energy: Barrier to Across Lipid Membranes

Lipophilic cations, such as TPPs, are lipid-soluble despite their positive charge. They can readily pass through the phospholipid bilayer into the mitochondria.[13] In contrast, hydrophilic cations, such as Na^+ and K^+, can across the plasma and mitochondrial transmembranes only with the help of ionophores or carrier proteins. The impermeability of biological membranes to hydrophilic cations is largely due to the high activation energy required to move them from an aqueous environment into the lipid core (Figure 8) of the membrane.[86] The activation energy is composed of two components: the repulsive electrostatic interactions and the attractive hydrophobic forces.[87] The main repulsive electrostatic energy component, Born energy, is due to the enthalpy required to overcome charge repulsion and to remove salvation water molecules from the cation upon transfer from aqueous environment to the lipid core of the membrane.[13, 88] The Born energy (W_B) is given by the following equation:

$$W_B = \frac{q^2}{8\pi\varepsilon_o r}\left(\frac{1}{\varepsilon_1}+\frac{1}{\varepsilon_2}\right) \overset{\varepsilon_1=2\,(\text{lipid}),\ \varepsilon_2=80\,(\text{water})}{\Rightarrow} \frac{339Z^2}{r}$$

where ε_o is the vacuum permittivity, ε_1 is the dielectric constant within the lipid core of the membrane (~2), ε_2 is the dielectric of water (~80), q is the charge per mole of cation, r is the ionic radius, and Z is the charge per cation.[13, 88] Born energy is decreased when cation becomes bigger (larger r value). The attractive component of activation energy is due to hydrophobicity of the cation (Figure 8). This energy is required to move an uncharged molecule with identical size and hydrophobicity from aqueous environment into lipid core of the phospholipid bilayer.[86, 87] This component of activation energy is attractive for lipophilic organic cations due to increased entropy (loss of water structure when moving a molecule into the lipid core). The combination of decreased Born energy due to their much larger size and high attractive hydrophobic effect might contribute to 10^7 – 10^8-fold faster permeation kinetics through the phospholipid bilayer for triphenylphosphonium cations (Figure 9) as compared to that of Na^+ and K^+.[87, 89]

Membrane Penetration Kinetics: Control of Tumor Selectivity

Another important factor influencing the radiotracer's tumor uptake and selectivity is mitochondrial density in different organs or tissues. Myocardium has the highest mitochondrial density and may occupy up to 40% of total volume of myocytes. Other mitochondrion-rich organs also include the salivary gland, liver and kidneys. For lipophilic cationic radiotracers (log P = 0.5 – 1.5), such as ^{99m}Tc-Sestamibi (log P = 1.1), their membrane diffusion kinetics are so fast that they tend to localize in the mitochondrion-rich organs, such as heart, liver, kidneys and salivary gland. For hydrophilic cations (log P = −1.0 – −3.0), such as ^{64}Cu(**6**) (log P = −1.7), the low lipophilicity makes it more difficult for them to across mitochondrial membranes,[63, 64] and often leads to a slow membrane diffusion kinetics; thereby forcing them to localize in tissues where the negative

mitochondrial potential is elevated. Thus, it is not surprising that ^{64}Cu(**6**) (log P = −1.7) and ^{64}Cu(**3**) (log P = −2.7) have excellent tumor selectivity (Figure 9) with very low uptake in the heart and muscle. In this respect, cationic radiotracers with log P values in the range of 0.5 – 1.3 are particularly useful for imaging organs (heart, liver and salivary gland) with high mitochondrial density due to their fast membrane-penetration kinetics. In contrast, cationic radiotracers with log P values in the range of −1.0 to −3.0 are best fitted for imaging tumors with the elevated mitochondrial potential. This conclusion is completely consistent with the results from pre-clinical studies on cationic anticancer drugs and triarylmethane dyes for their phototoxicity towards tumor cells.[90–94]

Optimal Lipophilicity

There is little information available with regard to the optimal lipophilicity for a radiotracer to achieve high tumor-selectivity. A predictive model has been reported for selective accumulation of generic chemicals in carcinoma tumor cells.[95] It was predicted that the optimal log P value for an organic cation to achieve high tumor selectivity is between 0.0 and −1.5. However, caution must be taken in using this predictive model because the molecular shape of ^{64}Cu-labeled cations is significantly different from that of their parent phosphonium cations. Based on the results from biodistribution studies in the glioma model, it seems that the optimal log P value for a ^{64}Cu-labeled phosphonium cation to achieve high tumor selectivity is between −1.0 and −3.0 (Figure 9). This conclusion should be further confirmed for other ^{64}Cu-labeled organic cations.

Subcellular Distribution Characteristics

To understand the tumor localization mechanism of ^{64}Cu-labeled phosphonium cations, subcellular distribution studies were performed on ^{64}Cu(**3**) and ^{64}Cu(**6**) using a standard differential centrifugation method.[63, 64] ^{99m}Tc-Sestamibi was used for comparison purposes since ^{99m}Tc-Sestamibi is widely used for imaging tumors in cancer patients. It was found that ^{64}Cu(**3**), ^{64}Cu(**6**) and ^{99m}Tc-Sestamibi share similar subcellular distribution patterns.[63, 64] Since it is well-accepted that ^{99m}Tc-Sestamibi is a mitochondrion-targeting cationic radiotracer, we believe that ^{64}Cu(**3**) and ^{64}Cu(**6**) are able to localize in the energized mitochondria of tumor cells, where the negative potential is significantly elevated.

^{64}Cu(DO3A-xy-ACR): A Close "Relative" of ^{64}Cu-Labeled Phosphonium Cations

To further demonstrate the mitochondrion-targeting capability of ^{64}Cu-labeled phosphonium cations, we recently evaluated ^{64}Cu(DO3A-xy-ACR) (Figure 10: DO3A-xy-ACR = 2,6-bis(dimethylamino)-10-(4-((4,7,10-tris(carboxymethyl)-1,4,7,10-tetraazacyclo-dodecan-1-yl)methyl)benzyl)acridin-10-ium) in the glioma-bearing animal model.[96] We also prepared Cu(DO3A-xy-ACR) for cell-staining assays. We found that ^{64}Cu(DO3A-xy-ACR) remained in the glioma for >24 h while Cu(DO3A-xy-ACR) was able to localize in the mitochondria of glioma cells (Figure 10). Although ^{64}Cu(DO3A-xy-ACR) is not an ideal PET radiotracer for tumor imaging due to its high liver uptake,[96] the results from this study provided strong indirect evidence to suggest that ^{64}Cu-labeled phosphonium cations are able to localize in the energized mitochondria of tumor cells, where the negative transmembrane potential is elevated.

Conclusion

^{64}Cu-labeled phosphonium cations are a new class of PET radiotracers with high tumor selectivity. While their high tumor uptake can be attributed to the enhanced mitochondrial potential, the tumor selectivity of ^{64}Cu-labeled phosphonium cations is most likely attributed to their low lipophilicity, and slow membrane-penetration kinetics. It is appreciated that ^{18}F-labeling of phosphonium cations usually results in minimal changes in

their physical and biological properties. In contrast, the radiolabeling of phosphonium cations with metallic radionuclide (such as ^{64}Cu, ^{99m}Tc and ^{111}In) requires the use of a BFC and results in significant changes in the molecular size, lipophilicity and biodistribution properties. Even though the exact structural requirements for radiometal chelates remain unknown, one thing is certain that attachment of the ^{64}Cu-DO3A chelate onto phosphonium cations results in radiotracers with good tumor uptake and high tumor selectivity. Among the ^{64}Cu-labeled phosphonium cations evaluated in the glioma-bearing animal model, ^{64}Cu(**6**) has the best tumor uptake with very high tumor selectivity. Future studies will be directed towards understanding of solution structures of radiometal (^{64}Cu, ^{99m}Tc and ^{111}In) chelates and their impact on cellular uptake kinetics of radiolabeled phosphonium cations.

Acknowledgments

The author would like to thank Dr. Xiaoyuan Chen at the National Institute of Biomedical Imaging and Bioengineering (NIBIB) for PET imaging studies. This work is supported, in part, by Purdue University and research grants: R01 CA115883 from National Cancer Institute (NCI).

ABBREVIATIONS

DO3A-bu-TPP (1)	triphenyl(4-((4,7,10-tris(carboxymethyl)-1,4,7,10-tetraazacyclododecan-1-yl)methyl)-3-propyl)phosphonium
DO3A-bu-TPP (2)	triphenyl(4-((4,7,10-tris(carboxymethyl)-1,4,7,10-tetraazacyclododecan-1-yl)methyl)-4-butyl)phosphonium
DO3A-xy-TPP (3)	triphenyl(4-((4,7,10-tris(carboxymethyl)-1,4,7,10-tetraazacyclododecan-1-yl)methyl)benzyl)phosphonium
DO3A-xy-TPA (4)	triphenyl(4-((4,7,10-tris(carboxymethyl)-1,4,7,10-tetraazacyclododecan-1-yl)methyl)benzyl)arsonium
DO3A-xy-mTPP (5)	tris(4-methoxyphenyl)(4-((4,7,10-tris(carboxymethyl)-1,4,7,10-tetraazacyclododecan-1-yl)methyl)benzyl)phosphonium
DO3A-xy-TPEP (6)	(2-(diphenylphosphoryl)ethyl)diphenyl(4-((4,7,10-tris(carboxymethyl)-1,4,7,10-tetraazacyclododecan-1-yl)methyl)benzyl)phosphonium
DO2A-xy-TPP (7)	(4-((4,10-bis(carboxymethyl)-1,4,7,10-tetraazacyclododecan-1-yl)methyl)benzyl)triphenylphosphonium
DO2A-(xy-TPP)$_2$ (8)	(4,4′-(4,10-bis(carboxymethyl)-1,4,7,10-tetraazacyclododecane-1,7-diyl)bis(methylene)bis(4,1-phenylene))bis(methylene)bis(triphenylphosphonium)
NOTA-Bn-xy-TPP (9)	triphenyl(4-((3-(4-((1,4,7,10-tetrakis(carboxymethyl)-1,4,7,10-tetraazacyclododecan-2-yl)methyl)phenyl)thioureido)methyl)benzyl)phosphonium
DOTA-Bn-xy-TPEP (10)	(2-(diphenylphosphoryl)ethyl)diphenyl(4-((3-(4-((1,4,7,10-tetrakis(carboxymethyl)-1,4,7,10-tetraazacyclododecan-2-yl)methyl)phenyl)thioureido)methyl)benzyl)phosphonium
NOTA-Bn-xy-TPEP (11)	(2-(diphenylphosphoryl)ethyl)diphenyl(4-((3-(4-((1,4,7-tris(carboxymethyl)-1,4,7-triazonan-2-yl)methyl)phenyl)thioureido)methyl)benzyl)phosphonium

and NOTA-Bn-xy-TPP (12)	triphenyl(4-((3-(4-((1,4,7-tris(carboxymethyl)-1,4,7-triazonan-2-yl)methyl)phenyl)thioureido)methyl)benzyl)phosphonium

References

1. Jemal A, Siegel R, Xu J, Ward E. Cancer statistics, 2010. CA Cancer J Clin. 2010; 60:277–300. [PubMed: 20610543]
2. Kroemer G, Dallaporta B, Resche-Rigon M. The mitochondrial death/life regulator in apoptosis and necrosis. Annu Rev Physiol. 1998; 60:619–642. [PubMed: 9558479]
3. Modica-Napolitano JS, Aprille JR. Delocalized lipophilic cations selectively target the mitochondria of carcinoma cells. Adv Drug Deliv Rev. 2001; 49:63–70. [PubMed: 11377803]
4. Duchen MR. Mitochondria in health and disease: perspectives on a new mitochondrial biology. Mol Aspects Med. 2004; 25:365–451. [PubMed: 15302203]
5. Modica-Napolitano JS, Singh KK. Mitochondria as targets for detection and treatment of cancer. Expert Rev Mol Med. 2002; 4:1–19. [PubMed: 14987393]
6. Johnson LV, Walsh ML, Chen LB. Localization of mitochondria in living cells with rhodamine 123. Proc Natl Acad Sci U S A. 1980; 77:990–994. [PubMed: 6965798]
7. Summerhayes IC, Lampidis TJ, Bernal SD, Nadakavukaren JJ, Nadakavukaren KK, Shepard EL, Chen LB. Unusual retention of rhodamine 123 by mitochondria in muscle and carcinoma cells. Proc Natl Acad Sci U S A. 1982; 79:5292–5296. [PubMed: 6752944]
8. Modica-Napolitano JS, Aprille JR. Basis for the selective cytotoxicity of rhodamine 123. Cancer Res. 1987; 47:4361–4365. [PubMed: 2886218]
9. Davis S, Weiss MJ, Wong JR, Lampidis TJ, Chen LB. Mitochondrial and plasma membrane potentials cause unusual accumulation and retention of rhodamine 123 by human breast adenocarcinoma-derived MCF-7 cells. J Biol Chem. 1985; 260:13844–13850. [PubMed: 4055760]
10. Dairkee SH, Hackett AJ. Differential retention of rhodamine 123 by breast carcinoma and normal human mammary tissue. Breast Cancer Res Treat. 1991; 18:57–61. [PubMed: 1854980]
11. Mannella CA. The relevance of mitochondrial membrane topology to mitochondrial function. Biochim Biophys Acta. 2006; 1762:140–147. [PubMed: 16054341]
12. Gottlieb E, Thompson CB. Targeting the mitochondria to enhance tumor suppression. Methods Mol Biol. 2003; 223:543–554. [PubMed: 12777750]
13. Ross MF, Kelso GF, Blaikie FH, James AM, Cochemé HM, Filipovska A, Da Ros T, Hurd TR, Smith RA, Murphy MP. Lipophilic triphenylphosphonium cations as tools in mitochondrial bioenergetics and free radical biology. Biochemistry (Mosc). 2005; 70:222–230. [PubMed: 15807662]
14. Jakobs S. High resolution imaging of live mitochondria. Biochim Biophys Acta. 2006; 1763:561–575. [PubMed: 16750866]
15. Lichtshtein D, Kaback HR, Blume AJ. Use of a lipophilic cation for determination of membrane potential in neuroblastoma-glioma hybrid cell suspensions. Proc Natl Acad Sci U S A. 1979; 76:650–654. [PubMed: 284390]
16. Hockings PD, Rogers PJ. The measurement of transmembrane electrical potential with lipophilic cations. Biochim Biophys Acta. 1996; 1282:101–106. [PubMed: 8679645]
17. Huang SG. Development of a high throughput screening assay for mitochondrial membrane potential in living cells. J Biomol Screen. 2002; 7:383–389. [PubMed: 12230893]
18. Lefevre C, Kang HC, Haugland RP, Malekzadeh N, Arttamangkul S, Haugland RP. Texas Red-X and rhodamine Red-X, new derivatives of sulforhodamine 101 and lissamine rhodamine B with improved labeling and fluorescence properties. Bioconjug Chem. 1996; 7:482–489. [PubMed: 8853462]
19. Lavis LD, Chao TY, Raines RT. Fluorogenic label for biomolecular imaging. ACS Chem Biol. 2006; 1:252–260. [PubMed: 17163679]

20. Mao C, Kisaalita WS. Determination of resting membrane potential of individual neuroblastoma cells (IMR-32) using a potentiometric dye (TMRM) and confocal microscopy. J Fluoresc. 2004; 14:739–743. [PubMed: 15649026]
21. Scaduto RC Jr, Grotyohann LW. Measurement of mitochondrial membrane potential using fluorescent rhodamine derivatives. Biophys J. 1999; 76:469–477. [PubMed: 9876159]
22. Hama Y, Urano Y, Koyama Y, Kamiya M, Bernardo M, Paik RS, Shin IS, Paik CH, Choyke PL, Kobayashi H. A target cell-specific activatable fluorescence probe for in vivo molecular imaging of cancer based on a self-quenched avidin-rhodamine conjugate. Cancer Res. 2007; 67:2791–2799. [PubMed: 17363601]
23. Glunde K, Foss CA, Takagi T, Wildes F, Bhujwalla ZM. Synthesis of 6′-*O*-lissamine-rhodamine B-glucosamine as a novel probe for fluorescence imaging of lysosomes in breast tumors. Bioconjug Chem. 2005; 16:843–851. [PubMed: 16029026]
24. Longmire MR, Ogawa M, Hama Y, Kosaka N, Regino CA, Choyke PL, Kobayashi H. Determination of optimal rhodamine fluorophore for in vivo optical imaging. Bioconjug Chem. 2008; 19:1735–1742. [PubMed: 18610943]
25. Yova D, Atlamazoglou V, Kavantzas N, Loukas S. Development of a fluorescence-based imaging system for colon cancer diagnosis using two novel rhodamine derivatives. Lasers Med Sci. 2000; 15:140–147.
26. Saha GB, Go RT, Maclntyre WJ. Radiopharmaceuticals for cardiovascular imaging. Int J Rad Appl Instrum B. 1992; 19:1–20. [PubMed: 1577608]
27. Jain D. Technetium-99m labeled myocardial perfusion imaging agents. Semin Nucl Med. 1999; 29:221–236. [PubMed: 10433338]
28. Acampa W, Di Benedetto C, Cuocolo A. An overview of radiotracers in nuclear cardiology. J Nucl Cardiol. 2000; 7:701–707. [PubMed: 11144485]
29. Dilsizian V. The role of myocardial perfusion imaging in vascular endothelial dysfunction. J Nucl Cardiol. 2000; 7:180–184. [PubMed: 10796009]
30. Beller GA, Zaret BL. Contributions of nuclear cardiology to diagnosis and prognosis of patients with coronary artery disease. Circulation. 2000; 101:1465–1478. [PubMed: 10736294]
31. Parker JA. Cardiac nuclear medicine in monitoring patients with coronary heart disease. Semin Nucl Med. 2001; 31:223–237. [PubMed: 11430529]
32. Herman LW, Sharma V, Kronauge JF, Barbarics E, Herman LA, Piwnica-Worms D. Novel hexakis(arenisonitrile)technetium(I) complexes as radioligands targeted to the multidrug resistance P-glycoprotein. J Med Chem. 1995; 38:2955–2963. [PubMed: 7636856]
33. Luker GD, Fracasso PM, Dobkin J, Piwnica-Worms D. Modulation of the multidrug resistance P-glycoprotein: detection with technetium-99m-sestamibi in vivo. J Nucl Med. 1997; 38:369–372. [PubMed: 9074520]
34. Liu Z, Stevenson GD, Barrett HH, Kastis GA, Bettan M, Furenlid LR, Wilson DW, Woolfenden JM. Imaging recognition of multidrug resistance in human breast tumors using ^{99m}Tc-labeled monocationic agents and a high-resolution stationary SPECT system. Nucl Med Biol. 2004; 31:53–65. [PubMed: 14741570]
35. Liu Z, Stevenson GD, Barrett HH, Furenlid LR, Wilson DW, Kastis GA, Bettan M, Woolfenden JM. Imaging recognition of inhibition of multidrug resistance in human breast cancer xenografts using ^{99m}Tc-labeled sestamibi and tetrofosmin. Nucl Med Biol. 2005; 32:573–583. [PubMed: 16026704]
36. Schomäcker K, Schicha H. Use of myocardial imaging agents for tumor diagnosis: a success story? Eur J Nucl Med. 2000; 27:1845–1863. [PubMed: 11189949]
37. Del Vecchio S, Salvatore M. ^{99}Tc-MIBI in the evaluation of breast cancer biology. Eur J Nucl Med Mol Imaging. 2004; 31(Suppl 1):S88–S96. [PubMed: 15105972]
38. Sharma V, Piwnica-Worms D. Metal complexes for therapy and diagnosis of drug resistance. Chem Rev. 1999; 99:2545–2560. [PubMed: 11749491]
39. Sharma V. Radiopharmaceuticals for assessment of multidrug resistance P-glycoprotein-mediated drug transport activity. Bioconjug Chem. 2004; 15:1464–1474. [PubMed: 15546216]

40. Sharma V, Piwnica-Worms D. Monitoring multidrug resistance P-glycoprotein drug transport activity with single-photon emission computed tomography and positron emission tomography radiopharmaceuticals. Top Curr Chem. 2005; 252:155–178.
41. Vaidyanathan G, Zalutsky MR. Imaging drug resistance with radiolabeled molecules. Curr Pharm Des. 2004; 10:2965–2979. [PubMed: 15379662]
42. Filippi L, Santoni R, Manni C, Danieli R, Floris R, Schillaci O. Imaging primary brain tumors by single-photon emission computerized tomography (SPECT) with technetium-99m Sestamibi (MIBI) and Tetrofosmin. Curr Med Imag Rev. 2005; 1:61–66.
43. Srivastava PC, Knapp FF Jr. [(*E*)-1-[^{123}I]Iodo-penten-5-yl]triphenylphosphonium iodide: convenient preparation of a potential useful myocardial perfusion agent. J Med Chem. 1984; 27:978–981. [PubMed: 6747996]
44. Srivastava PC, Hay HG, Knapp FF Jr. Effects of alkyl and aryl substitution on the myocardial specificity of radioiodinated phosphonium, arsonium, and ammonium cations. J Med Chem. 1985; 28:901–904. [PubMed: 4009613]
45. Krause BJ, Szabo Z, Becker LC, Dannals RF, Scheffel U, Seki C, Ravert HT, Dipaola AF Jr, Wagner HN Jr. Myocardial perfusion with [^{11}C]methyl triphenyl phosphonium: measurements of the extraction fraction and myocardial uptake. J Nucl Biol Med. 1994; 38:521–526. [PubMed: 7865551]
46. Madar I, Anderson JH, Szabo Z, Scheffel U, Kao PF, Ravert HT, Dannals RF. Enhanced uptake of [^{11}C]TPMP in canine brain tumor: a PET study. J Nucl Med. 1999; 40:1180–1185. [PubMed: 10405140]
47. Madar I, Weiss L, Izbicki G. Preferential accumulation of ^{3}H-tetraphenylphosphonium in non-small cell lung carcinoma in mice: comparison with ^{99m}Tc-MIBI. J Nucl Med. 2002; 43:234–238. [PubMed: 11850490]
48. Ravert HT, Madar I, Dannals RF. Radiosynthesis of 3-[^{18}F]fluoropropyl and 4-[^{18}F]fluorobenzyl triarylphosphonium ions. J Label Compd Radiopharm. 2004; 47:469–476.
49. Madar I, Ravert HT, Du Y, Hilton J, Volokh L, Dannals RF, Frost JJ, Hare JM. Characterization of uptake of the new PET imaging compound ^{18}F-fluorobenzyl triphenyl phosphonium in dog myocardium. J Nucl Med. 2006; 47:1359–1366. [PubMed: 16883017]
50. Cheng Z, Subbarayan M, Chen X, Gambhir SS. Synthesis of (4-[^{18}F]fluorophenyl)triphenylphosphonium as a potential imaging agent for mitochondrial dysfunction. J Label Compd Radiopharm. 2005; 48:131–137.
51. Cheng Z, Winant RC, Gambhir SS. A new strategy to screen molecular imaging probe uptake in cell culture without radiolabeling using matrix-assisted laser desorption/ionization time-of-flight mass spectrometry. J Nucl Med. 2005; 46:878–886. [PubMed: 15872363]
52. Min JJ, Biswal S, Deroose C, Gambhir SS. Tetraphenylphosphonium as a novel molecular probe for imaging tumors. J Nucl Med. 2004; 45:636–643. [PubMed: 15073261]
53. Steichen JD, Weiss MJ, Elmaleh DR, Martuza RL. Enhanced in vitro uptake and retention of ^{3}H-tetraphenylphosphonium by nervous system tumor cells. J Neurosurg. 1991; 74:116–122. [PubMed: 1984490]
54. Anderson, CJ.; Green, MA.; Fujibayashi, Y. Chemistry of copper radionuclides and radiopharmaceutical products. In: Welch, MJ.; Redvanly, C., editors. Handbook of Radiopharmaceuticals: Radiochemistry and Applications. John Wiley & Sons, Ltd; 2003. p. 401-422.
55. Smith SV. Molecular imaging with copper-64. J Inorg Biochem. 2004; 98:1874–1901. [PubMed: 15522415]
56. Blower PJ, Lewis JS, Zweit J. Copper radionuclides and radiopharmaceuticals in nuclear medicine. Nucl Med Biol. 1996; 23:957–980. [PubMed: 9004284]
57. Liu S. The role of coordination chemistry in development of target-specific radiopharmaceuticals. Chem Soc Rev. 2004; 33:1–18. [PubMed: 14737504]
58. Reichert DE, Lewis JS, Anderson CJ. Metal complexes as diagnostic tools. Coord Chem Rev. 1999; 184:3–66.
59. Anderson CJ, Welch MJ. Radiometal-labeled agents (non-technetium) for diagnostic imaging. Chem Rev. 1999; 99:2219–2234. [PubMed: 11749480]

60. Liu S. Bifunctional coupling agents for radiolabeling of biomolecules and target-specific delivery of metallic radionuclides. Adv Drug Deliv Rev. 2008; 60:1347–1370. [PubMed: 18538888]
61. Wang J, Yang CT, Kim YS, Sreerama SG, Cao Q, Li ZB, He Z, Chen X, Liu S. ^{64}Cu-labeled triphenylphosphonium and triphenylarsonium cations as highly tumor-selective imaging agents. J Med Chem. 2007; 50:5057–5069. [PubMed: 17867662]
62. Yang CT, Li Y, Liu S. Synthesis and structural characterization of complexes of a DO3A-conjugated triphenylphosphonium cation with diagnostically important metal ions. Inorg Chem. 2007; 46:8988–8997. [PubMed: 17784751]
63. Kim YS, Yang CT, Wang J, Wang L, Li ZB, Chen X, Liu S. Effects of targeting moiety, linker, bifunctional chelator, and molecular charge on biological properties of ^{64}Cu-labeled triphenylphosphonium cations. J Med Chem. 2008; 51:2971–2984. [PubMed: 18419113]
64. Yang CT, Kim YS, Wang J, Wang L, Shi J, Li ZB, Chen X, Fan M, Li JJ, Liu S. ^{64}Cu-labeled 2-(Diphenylphosphoryl)ethyldiphenylphosphonium cations as highly selective tumor imaging agents: effects of linkers and chelates on radiotracer biodistribution characteristics. Bioconjug Chem. 2008; 19:2008–2022. [PubMed: 18763821]
65. Liu S, Kim YS, Zhai S, Shi J, Hou G. Evaluation of ^{64}Cu(DO3A-xy-TPEP) as a potential PET radiotracer for monitoring tumor multidrug resistance. Bioconjug Chem. 2009; 20:790–798. [PubMed: 19284752]
66. Deshpande SV, DeNardo SJ, Meares CF, McCall MJ, Adams GP, Moi MK, DeNardo GL. Copper-67-labeled monoclonal antibody Lym-1, a potential radiopharmaceutical for cancer therapy: labeling and biodistribution in RAJI tumored mice. J Nucl Med. 1988; 29:217–225. [PubMed: 3258025]
67. Anderson CJ, Pajeau TS, Edwards WB, Sherman EL, Rogers BE, Welch MJ. In vitro and in vivo evaluation of copper-64-octreotide conjugates. J Nucl Med. 1995; 36:2315–2325. [PubMed: 8523125]
68. Anderson CJ, Jones LA, Bass LA, Sherman EL, McCarthy DW, Cutler PD, Lanahan MV, Cristel ME, Lewis JS, Schwarz SW. Radiotherapy, toxicity and dosimetry of copper-64-TETA-octreotide in tumor-bearing rats. J Nucl Med. 1998; 39:1944–1951. [PubMed: 9829587]
69. Lewis JS, Srinivasan A, Schmidt MA, Anderson CJ. In vitro and in vivo evaluation of ^{64}Cu-TETA-Tyr^3-octreotate. A new somatostatin analog with improved target tissue uptake. Nucl Med Biol. 1999; 26:267–273. [PubMed: 10363797]
70. Lewis JS, Lewis MR, Cutler PD, Srinivasan A, Schmidt MA, Schwarz SW, Morris MM, Miller JP, Anderson CJ. Radiotherapy and dosimetry of ^{64}Cu-TETA-Tyr^3-octreotate in a somatostatin receptor-positive, tumor-bearing rat model. Clin Cancer Res. 1999; 5:3608–3616. [PubMed: 10589778]
71. Chen X, Liu S, Hou Y, Tohme M, Park R, Bading JR, Conti PS. MicroPET imaging of breast cancer α_v-integrin expression with ^{64}Cu-labeled dimeric RGD peptides. Mol Imaging Biol. 2004; 6:350–359. [PubMed: 15380745]
72. Wu Y, Zhang X, Xiong Z, Cheng Z, Fisher DR, Liu S, Gambhir SS, Chen X. MicroPET imaging of glioma integrin $\alpha_v\beta_3$ expression using ^{64}Cu-labeled tetrameric RGD peptide. J Nucl Med. 2005; 46:1707–1718. [PubMed: 16204722]
73. McQuade P, Miao Y, Yoo J, Quinn TP, Welch MJ, Lewis JS. Imaging of melanoma using ^{64}Cu- and ^{86}Y-DOTA-ReCCMSH(Arg^{11}), a cyclized peptide analogue of α-MSH. J Med Chem. 2005; 48:2985–2992. [PubMed: 15828837]
74. Shi J, Kim YS, Zhai S, Liu Z, Chen X, Liu S. Improving tumor uptake and pharmacokinetics of ^{64}Cu-labeled cyclic RGD peptide dimers with Gly_3 and PEG_4 linkers. Bioconjug Chem. 2009; 20:750–759. [PubMed: 19320477]
75. Prasanphanich AF, Nanda PK, Rold TL, Ma L, Lewis MR, Garrison JC, Hoffman TJ, Sieckman GL, Figueroa SD, Smith CJ. [^{64}Cu-NOTA-8-Aoc-BBN(7–14)NH_2] targeting vector for positron-emission tomography imaging of gastrin- releasing peptide receptor-expressing tissues. Proc Natl Acad Sci U S A. 2007; 104:12462–12467. [PubMed: 17626788]
76. Garrison JC, Rold TL, Sieckman GL, Figueroa SD, Volkert WA, Jurisson SS, Hoffman TJ. In vivo evaluation and small-animal PET/CT of a prostate cancer mouse model using ^{64}Cu bombesin

analogs: side-by-side comparison of the CB-TE2A and DOTA chelation systems. J Nucl Med. 2007; 48:1327–1337. [PubMed: 17631556]

77. Kumar K, Tweedle MF, Malley MF, Gougoutas JZ. Synthesis, stability, and crystal structure studies of some Ca^{2+}, Cu^{2+}, and Zn^{2+} complexes of macrocyclic polyamino carboxylates. Inorg Chem. 1995; 34:6472–6480.
78. Boswell CA, Sun X, Niu W, Weisman GR, Wong EH, Rheingold AL, Anderson CJ. Comparative in vivo stability of copper-64-labeled cross-bridged and conventional tetraazamacrocyclic complexes. J Med Chem. 2004; 47:1465–1474. [PubMed: 14998334]
79. Boswell CA, McQuade P, Weisman GR, Wong EH, Anderson CJ. Optimization of labeling and metabolite analysis of copper-64-labeled azamacrocyclic chelators by radio-LC-MS. Nucl Med Biol. 2005; 32:29–38. [PubMed: 15691659]
80. Sprague JE, Peng Y, Fiamengo AL, Woodin KS, Southwick EA, Weisman GR, Wong EH, Golden JA, Rheingold AL, Anderson CJ. Synthesis, characterization and in vivo studies of Cu(II)-64-labeled cross-bridged tetraazamacrocycle-amide complexes as models of peptide conjugate imaging agents. J Med Chem. 2007; 50:2527–2535. [PubMed: 17458949]
81. Bass LA, Wang M, Welch MJ, Anderson CJ. In vivo transchelation of copper-64 from TETA-octreotide to superoxide dismutase in rat liver. Bioconjug Chem. 2000; 11:527–532. [PubMed: 10898574]
82. Anderson CJ. Metabolism of radiometal-labeled proteins and peptides: what are the real radiopharmaceuticals in vivo? Cancer Biother Radiopharm. 2001; 16:451–455. [PubMed: 11789022]
83. Le Jeune N, Perek N, Denoyer D, Dubois F. Influence of glutathione depletion on plasma membrane cholesterol esterification and on Tc-99m-sestamibi and Tc-99m-tetrofosmin uptakes: a comparative study in sensitive U-87-MG and multidrug-resistant MRP1 human glioma cells. Cancer Biother Radiopharm. 2004; 19:411–421. [PubMed: 15453956]
84. Bähr O, Rieger J, Duffner F, Meyermann R, Weller M, Wick W. P-glycoprotein and multidrug resistance-associated protein mediate specific patterns of multidrug resistance in malignant glioma cell lines, but not in primary glioma cells. Brain Pathol. 2003; 13:482–494. [PubMed: 14655754]
85. Nakatsu S, Kondo S, Kondo Y, Yin D, Peterson JW, Kaakaji R, Morimura T, Kikuchi H, Takeuchi J, Barnett GH. Induction of apoptosis in multi-drug resistant (MDR) human glioblastoma cells by SN-38, a metabolite of the camptothecin derivative CPT-11. Cancer Chemother Pharmacol. 1997; 39:417–423. [PubMed: 9054955]
86. Ketterer B, Neumcke B, Läuger P. Transport mechanism of hydrophobic ions through lipid bilayer membranes. J Membrane Biol. 1971; 5:225–245.
87. Flewelling RF, Hubbel WL. Hydrophobic ion interactions with membranes. Thermodynamic analysis of tetraphenylphosphonium binding to vesicles. Biophy J. 1986; 49:531–540.
88. Honig BH, Hubell WL, Flewelling RF. Electrostatic interactions in membranes and proteins. Annu Rev Biophys Biophys Chem. 1986; 15:163–193. [PubMed: 2424473]
89. Grunwald E, Baughman G, Kohnstam G. The solvation of electrolytes in dioxane-water mixtures, as deduced from the effect of solvent change on the standard partial molar free energy. J Am Chem Soc. 1960; 82:5801–5811.
90. Kandela IK, Lee W, Indig GL. Effect of the lipophilic/hydrophilic character of cationic triarylmethane dyes on their selective phototoxicity toward tumor cells. Biotech Histochem. 2003; 78:157–169. [PubMed: 14714879]
91. Kandela K, Bartlett JA, Indig GL. Effect of molecular structure on the selective phototoxicity of triarylmethane dyes towards tumor cells. Photochem Photobiol Sci. 2002; 1:309–314. [PubMed: 12653467]
92. Horobin RW. Uptake, distribution, and accumulation of dyes and fluorescent probes within living cells. A structure-activity modeling approach. Adv Colour Sci Technol. 2001; 4:101–107.
93. Fantin VR, Beradi MJ, Scorrano L, Korsmeyer SJ, Leder P. A novel mitochondriotoxic small molecule that selectively inhibits tumor cell growth. Cancer Cell. 2002; 2:29–42. [PubMed: 12150823]
94. Britten CD, Rowinsky EK, Baker SD, Weiss GR, Smith L, Stephenson J, Rothenberg M, Smetzer L, Cramer J, Collins W, Von Hoff DD, Eckhardt SG. A phase I and pharmacokinetic study of the

mitochondrial-specific rhodacyanine dye analog MKT 077. Clin Cancer Res. 2000; 6:42–49. [PubMed: 10656430]

95. Trapp S, Horobin RW. A predictive model for the selective accumulation of chemicals in tumor cells. Eur Biophys J. 2005; 34:959–966. [PubMed: 15895221]
96. Zhou Y, Kim YS, Shi J, Chen X, Liu S. Evaluation of ^{64}Cu-labeled acridinium cation as potential PET radiotracer for tumor imaging. Bioconjug Chem. (unpublished results).

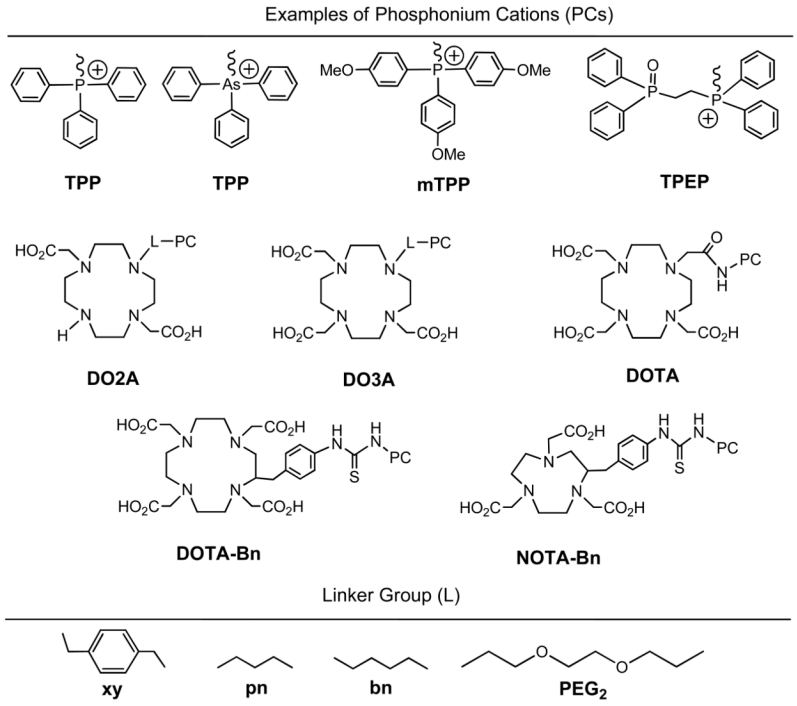

Figure 1.

Phosphonium cation conjugates for preparation of ^{64}Cu radiotracers. The phosphonium cation (PC) is used as the mitochondrion-targeting biomolecule to carry ^{64}Cu into the tumor cells where the negative mitochondrial potential is elevated as compared to normal cells. DOTA, DO3A, DO2A, NOTA and their derivatives are used as BFCs for ^{64}Cu chelation. Different linkers (L) are useful for modification of pharmacokinetics of ^{64}Cu radiotracers.

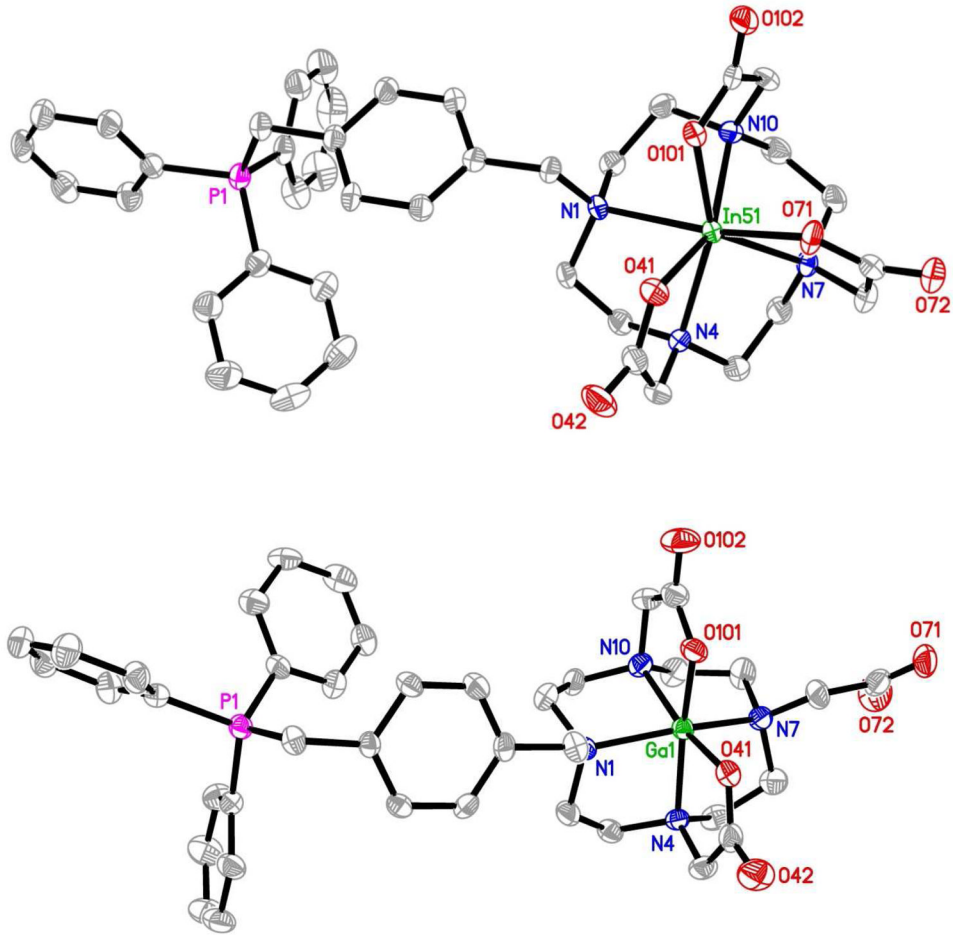

Figure 2.

ORTEP drawings of In(**3**)$^{+}$ (top) and Ga(**3**)$^{+}$ (bottom). Crystallization water molecules and hydrogen atoms are omitted for the sake of clarity. The structure of Mn(**3**) is almost identical to that of In(**3**)$^{+}$ despite their difference in the overall molecular charge.

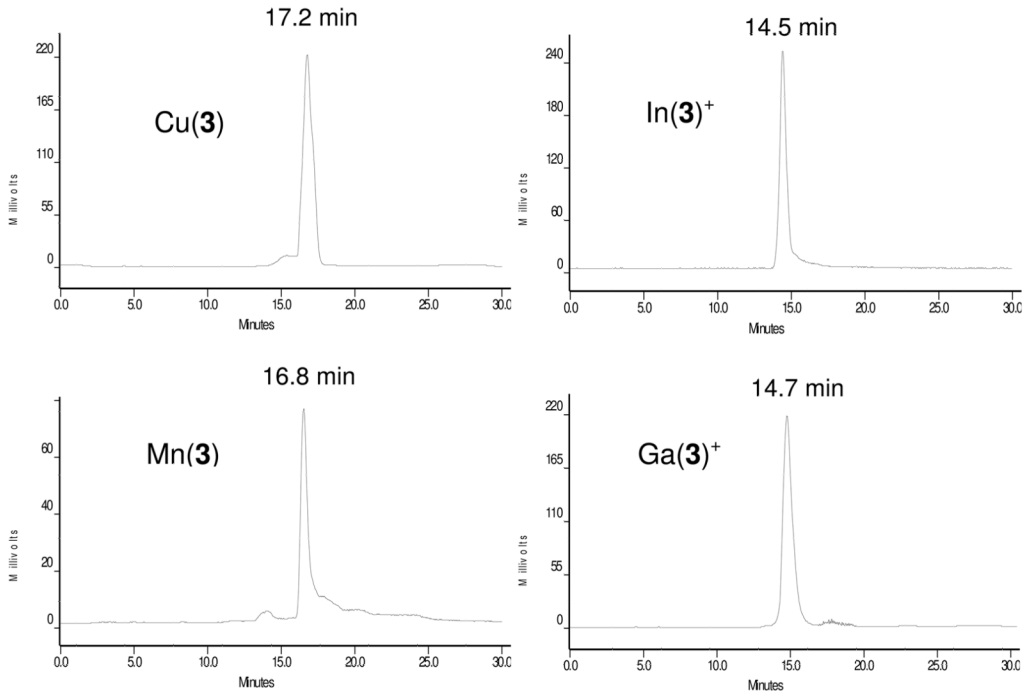

Figure 3.

Typical HPLC chromatograms of Cu(**3**), Mn(**3**), In(**3**)$^+$ and Ga(**3**)$^+$. The presence of a single peak suggests that they exist in solution as a single or "averaged" species. Obviously, Ga(**3**)$^+$ (14.7 min) and In(**3**)$^+$ (14.5 min) with the +1 overall molecular charge are more hydrophilic than Mn(**3**) (16.8 min) and Cu(**3**) (17.2 min) in their Zwitterion forms.

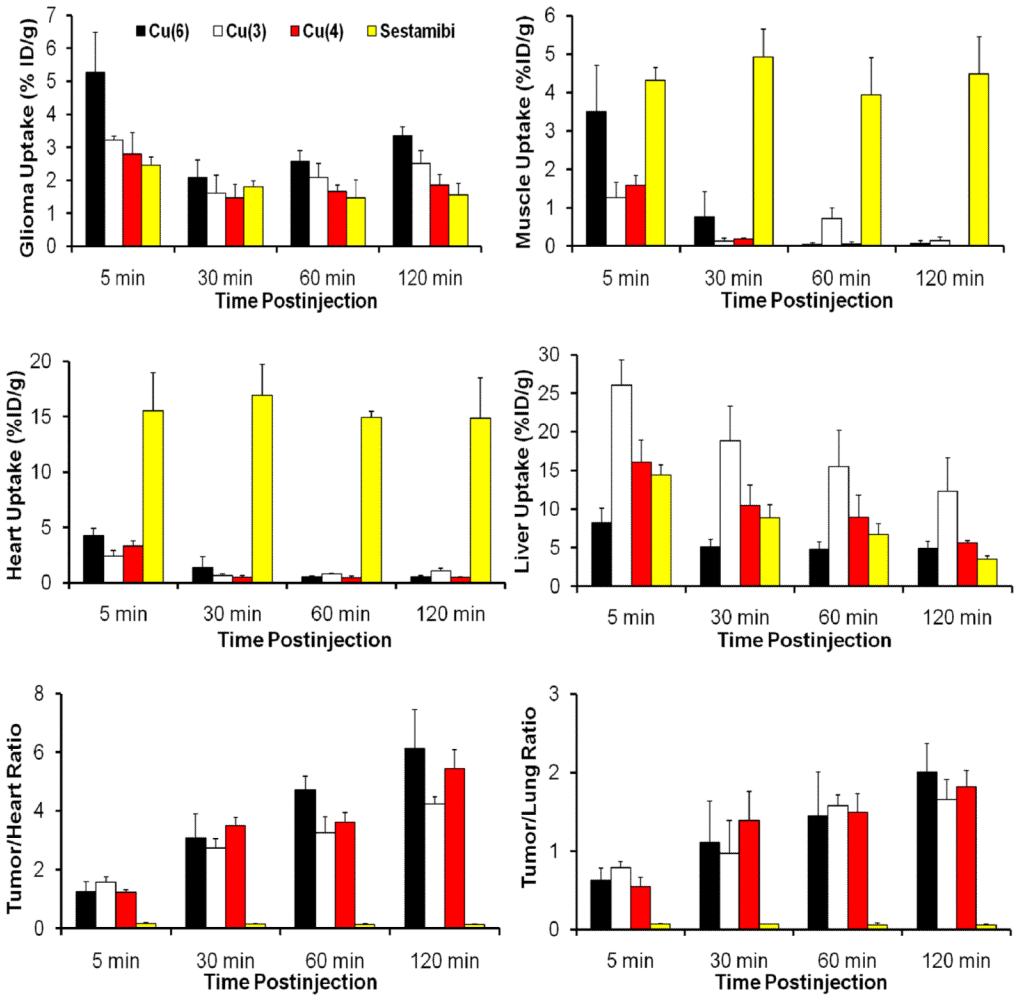

Figure 4.

Comparison between the ^{64}Cu-labeled phosphonium cations and ^{99m}Tc-Sestamibi with respect to their uptake in the glioma tumor, heart, liver and muscle, as well as their tumor/heart and tumor/lung ratios in the athymic nude mice bearing U87MG glioma xenografts.

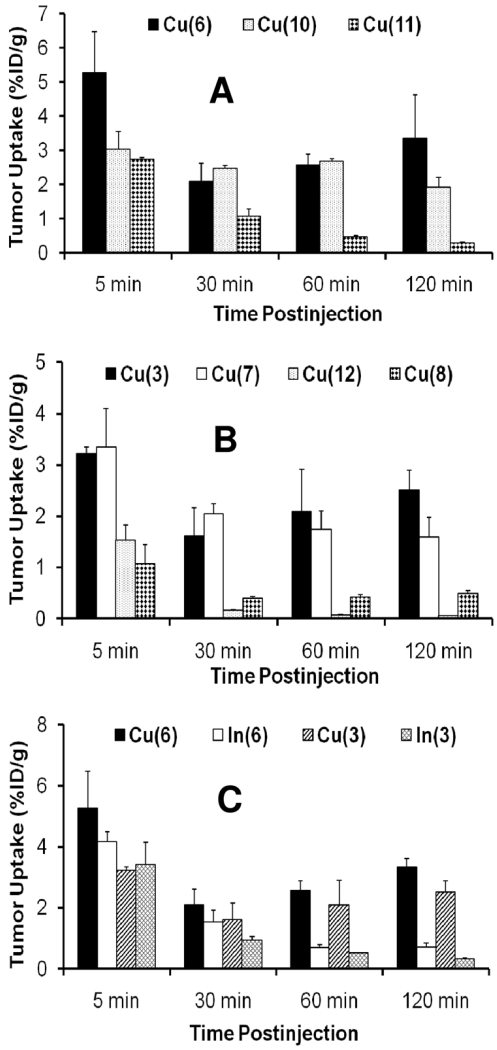

Figure 5.

Histograms to illustrate impacts of BFCs, overall charge and radiometal on the tumor uptake of ^{64}Cu and ^{111}In-labeled phosphonium cations in the athymic nude mice bearing U87MG human glioma xenografts.

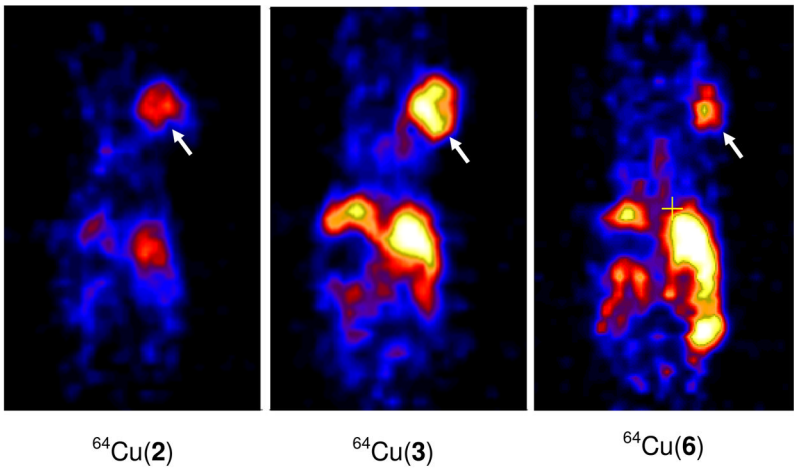

Figure 6.
Representative microPET images of the glioma-bearing mice administered with ~250 μCi of ^{64}Cu(**2**), ^{64}Cu(**3**) and ^{64}Cu(**6**) at 4 h p.i. Arrows indicate the presence of tumors.

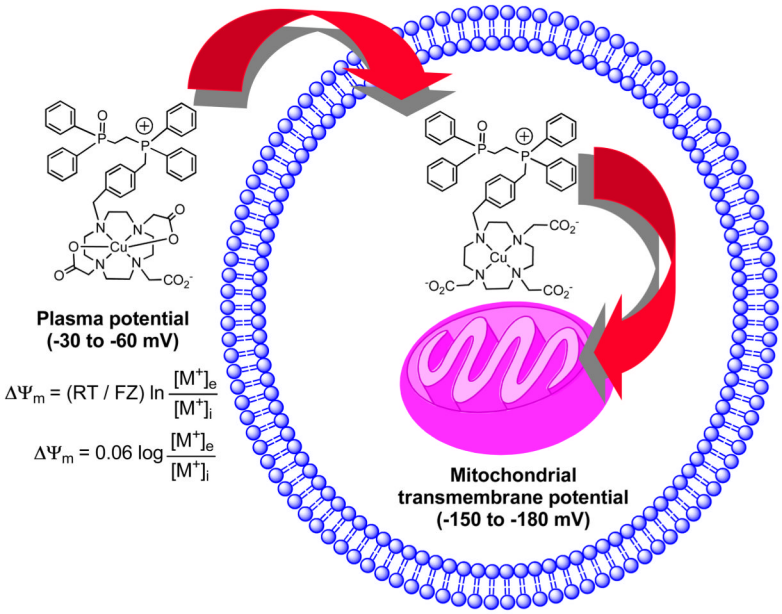

Figure 7.

Schematic presentation of the process for ^{64}Cu(**6**) to across the plasma and mitochondrial membranes. The main difference between tumor cells and normal cells is the mitochondrial potential. The difference in mitochondrial potential ($\Delta\psi_m$) between carcinoma cells and epithelial cells is ~60 mV, which contributes to ~10-fold more accumulation of ^{64}Cu(**6**) in mitochondria according to the Nernst equation. The plasma potential (−30 – −60 mV) also pre-concentrates ^{64}Cu(**6**) in the plasma. The lower pH value (pH = 4.5 – 5.0) inside tumor cells makes it easier for the two acetate chelating arms to become dissociated from ^{64}Cu.

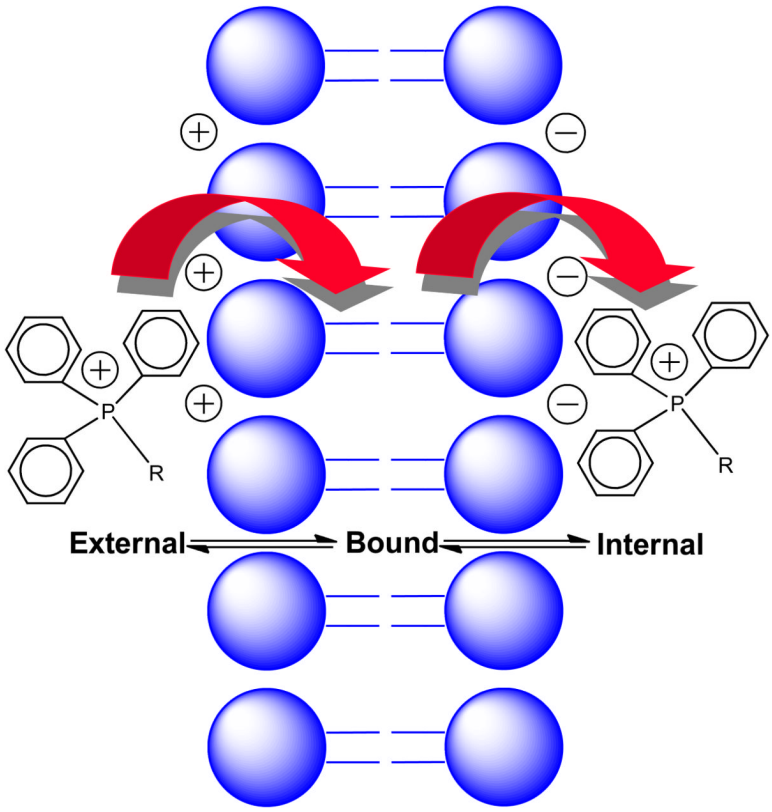

Figure 8.

Schematic illustration to move a triphenylphosphonium cation across a lipophilic membrane. The electrostatic interaction between the triphenylphosphonium cation and positive charges outside the membrane is repulsive. This component of activation energy is due to the enthalpy input required to overcome charge repulsion and to remove salvation water molecules from the cation upon transfer into the membrane lipid core. In contrast, the hydrophobic interaction between the triphenylphosphonium cation and lipid core is attractive due to hydrophobicity of the lipophilic phosphonium cation and increased entropy (loss of water structure when moving a molecule into the lipid core).

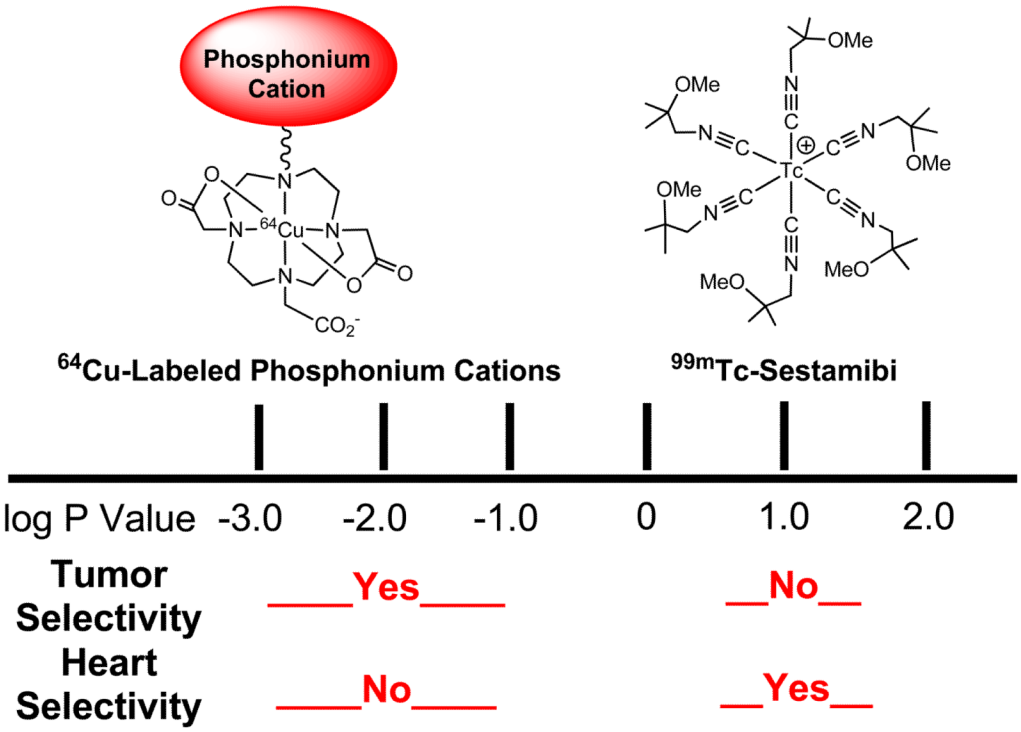

Figure 9.

Schematic presentation to illustrate the selectivity of cationic radiotracers based on their lipophilicity. ^{99m}Tc-Sestamibi is lipophilic (log P = 1.1), and its membrane diffusion rate is so fast that it can readily localize in mitochondrion-rich, such as the heart, liver and kidneys. The ^{64}Cu-labeled phosphonium cations, such as ^{64}Cu(**3**), are very hydrophilic (log P = −1.5 – −2.7) due to the hydrophilic ^{64}Cu-DO3A chelate. The slow diffusion kinetics makes it difficult for the ^{64}Cu-labeled phosphonium cations to across plasma and mitochondrial membranes, thereby forcing them to localize in the tumor where mitochondrial potential is elevated (~60 mV). While the enhanced negative mitochondrial potential provides the thermodynamic driving force for the ^{64}Cu-labeled phosphonium cations to localize in energized mitochondria of tumor cells, the hydrophilicity offers a control of their cell-penetrating kinetics and tumor selectivity.

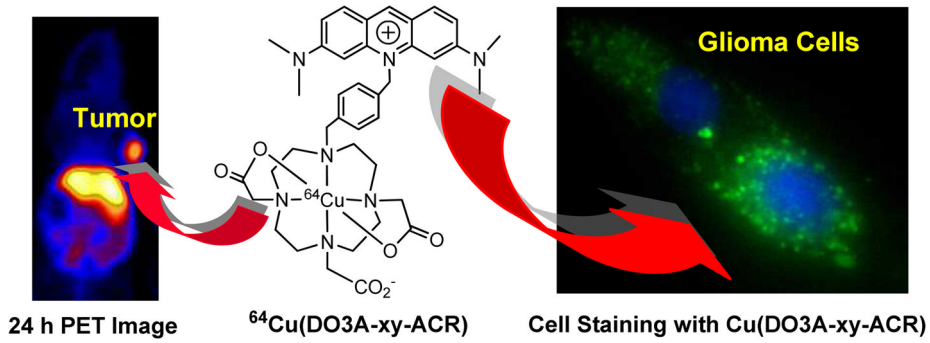

Figure 10.

Schematic presentation to show capability of ^{64}Cu(DO3A-xy-ACR) to localize in glioma. ^{64}Cu(DO3A-xy-ACR) is the PET radiotracer for tumor imaging while Cu(DO3A-xy-ACR) is used as the fluorescent probe to demonstrate their mitochondrial localization. The results from this study provided strong indirect evidence to suggest that ^{64}Cu-labeled phosphonium cations are able to localize in the energized mitochondria of tumor cells.

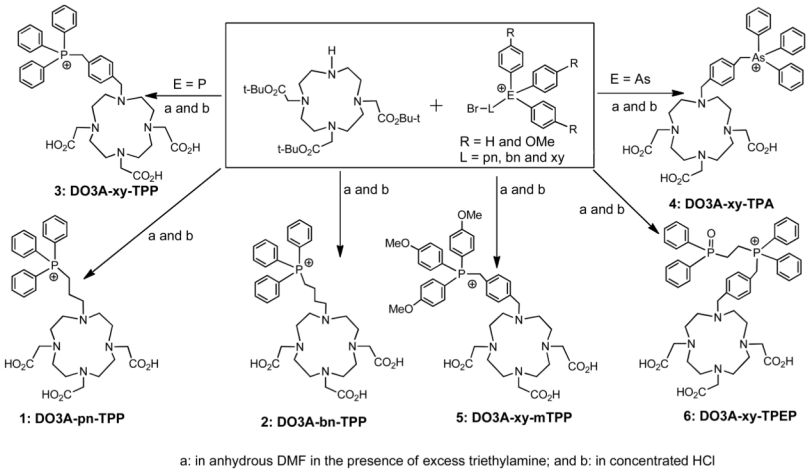

Chart I.
Synthesis of DO3A Conjugates.

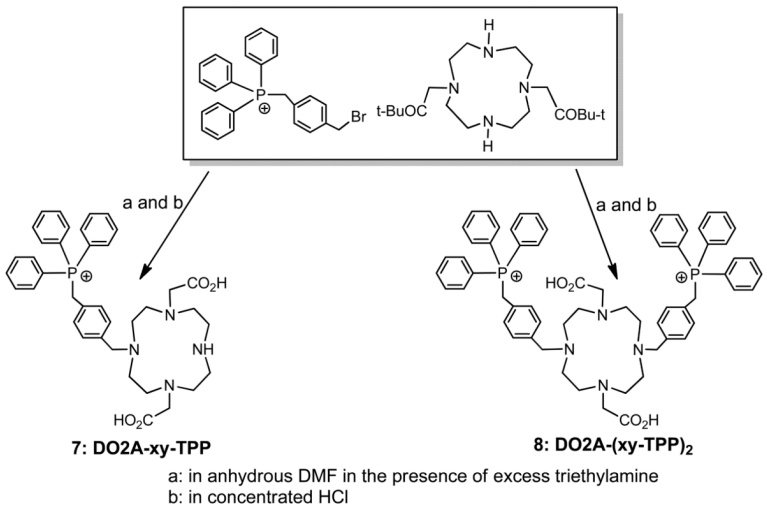

Chart II.
Synthesis of DO2A Conjugates.

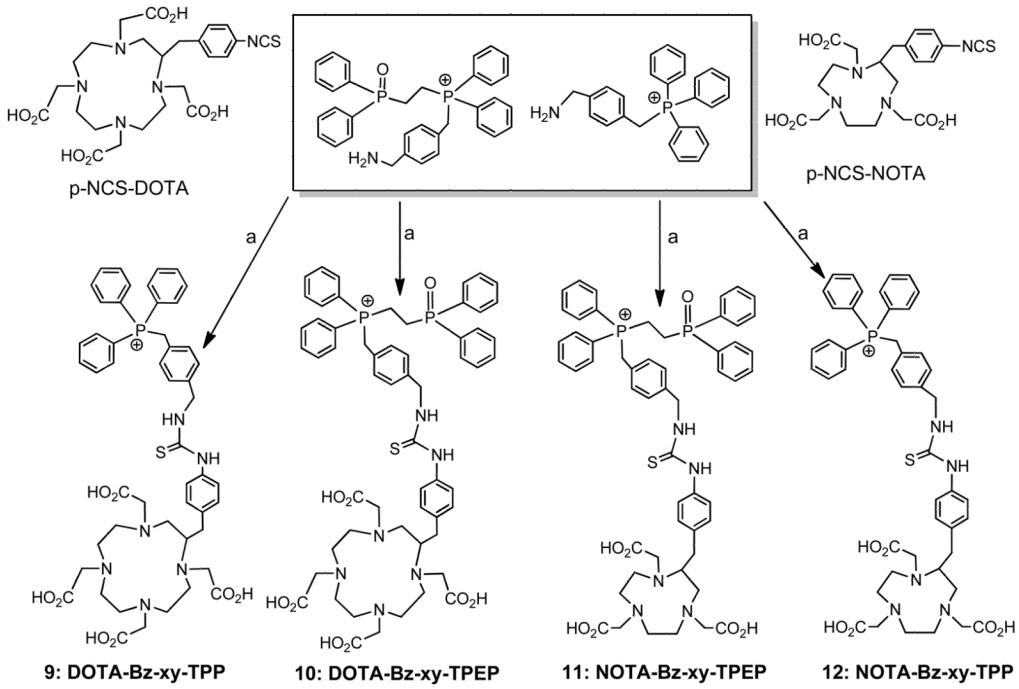

Chart III.
Synthesis of DOTA and NOTA Conjugates